LA-UR-14-26153
Approved for public release; distribution is unlimited.

Title: Quantitative MD simulations to assess UO2 thermal conductivity as a function of burnup

Author(s): Liu, Xiang-Yang
Andersson, Anders David Ragnar
Stanek, Christopher Richard

Intended for: Report

Issued: 2014-08-04

Quantitative MD simulations to assess UO_2 thermal conductivity as a function of burnup

X.-Y. Liu, C. R. Stanek, D. A. Andersson
Los Alamos National Laboratory, Los Alamos, NM 87545

1. Introduction

This milestone report highlights research activities towards quantitative molecular dynamics (MD) simulations to help assess degradation of oxide fuel, UO_2, thermal conductivity with burnup. The thermal conductivity of oxide fuel is an important materials property that affects the fuel performance since it is a key parameter that determines the temperature distribution of fuels, thus governing, e.g., dimensional changes due to thermal expansion, fission gas release rates, etc. The thermal conductivity of UO_2 nuclear fuel is also affected by fission gas, fission products, defects, and microstructural features such as grain boundaries. In this work, we report MD simulations to determine quantitatively, the effect of two fission products, Xe and La, on the thermal conductivity of UO_2, as a function of fission products concentrations, for a range of temperatures, 100 – 1500 K. Such effort closely follows earlier works on MD simulations of thermal conductivity in UO_2 [1, 2]. These results will be used to develop enhanced continuum thermal conductivity models for MARMOT and BISON with INL. These models will express the thermal conductivity as a function of state-variables, thus enabling thermal conductivity models with closer connection to the physical state of the fuel.

2. Computational methods

In non-metallic solids, phonons dominate thermal transport. This provides the basis of the MD based methodology to predict the thermal conductivity of these materials. Here, we have employed the non-equilibrium MD method, which is often referred to as the "direct method" [3-5]. In this method, a heat current (J) is applied to the

system, and the thermal conductivity κ is computed from the time-averaged temperature gradient ($\partial T / \partial z$) from Fourier's law,

$$\kappa = -\frac{J}{\partial T / \partial z} \tag{1}$$

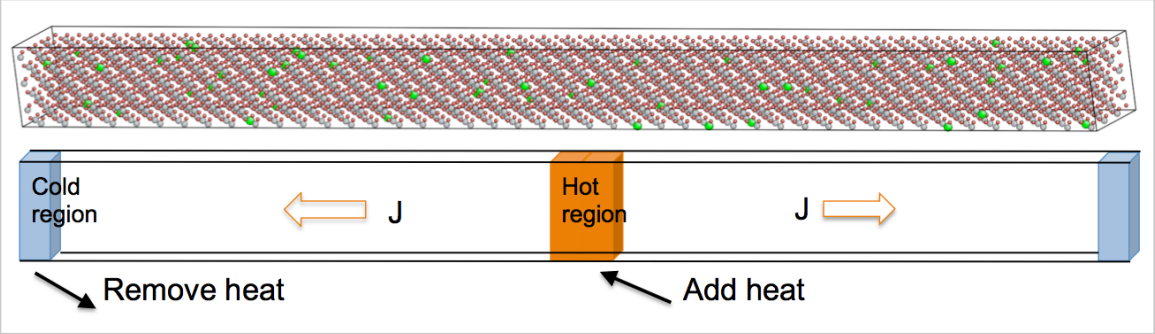

Figure 1. A schematic drawing that illustrates the computational setup of non-equilibrium MD simulations of thermal conductivity in UO_2 with fission products.

In Figure 1, the computational setup is illustrated. A supercell containing $n_1 \times n_2 \times n_3$ cubic unit cells of UO_2 is constructed. Periodic boundaries are applied in all three dimensions. The heat flow is in the z direction. A cold / hot region is defined at z = 0 / $L_z/2$ with 1 nm in width from which heat is removed / added during the simulations, where L_z is the periodic length of the supercell in the z direction. For all MD simulations, n_1 and n_2 are set to 3. The dependence of the computed thermal conductivity on cross sectional area has been shown to be weak [6]. The length L_z in the heat flow direction ranges from 19 to 76 nm for different cases.

In this work, the thermal conductivity calculations were carried out with the direct method as implemented in LAMMPS package [7]. The system is equilibrated initially for 50 ps in the NVT (constant number, constant volume, and constant temperature) ensemble at desired temperature, followed by another 50 ps in the NVE (constant number, constant volume, and constant energy) ensemble. After that, non-equilibrium MD runs were applied to the system, for a period of 5 – 10 ns. After thermal equilibration, the initial 0.5 ns in the thermal simulation was used to accommodate the transient behavior. After that, the temperature profiles were averaged over the rest of the MD time. There are two types of heat control methods in LAMMPS. One is based on the Muller-Plathe algorithm [4]. In this algorithm, the swap between the coldest particle in the cold region and the hottest atom in the hot region is used to remove / add heats to the

corresponding regions. By controlling the frequency of swaps during MD, the heat flux between the hot and the cold regions is controlled at the desired level. The other heat control algorithm is based on the method of Jund and Jullien [3]. In this scheme, a fixed amount of energy (ΔE) is added / subtracted from the hot / cold region by velocity rescaling every time step while preserving the total momentum ($\vec{P} = \sum_{i=1,N} m_i \vec{V}_i$) of the atoms in the region, so that

$$\vec{V}_i^{New} = \vec{V}_i + (1-\alpha)\frac{\vec{P}}{\sum m_i} \tag{2}$$

$$\alpha = \sqrt{1 \pm \frac{\Delta E}{E_k - \frac{1}{2}\sum m_i V_G^2}} \; ; \; V_G = \frac{\left|\vec{P}\right|}{\sum m_i} \tag{3}$$

The original Jund and Jullien algorithm was derived for single species system. We found that it applies to multiple species systems as well. Another constant heat flux algorithm using velocity rescaling from Ikeshoji and Hafskjold [5], which was originally derived for multiple species system is also widely used. These two algorithms are not equivalent, reflecting different flavors in the formulation since the mathematical solution of constant energy change while preserving momentum in a given region is not unique. We found that a precise control of the heat flux is important for studying the length dependence of the thermal conductivity. However, the control of the heat flux by using Muller-Plathe algorithm for given swap frequency is not good since the result depends on other simulation conditions. For this reason, the method of Jund and Jullien is adopted in all our MD simulations. The heat flux used in the simulations is 0.001 – 0.002 eV/*A* per time step, where *A* is the cross section area of the simulation cell.

The Buckingham type of empirical potential is used to describe the U^{4+} - O^{2-} [8], O^{2-} - O^{2-} [9] interactions in UO_2, as well as the Xe^0 - U^{4+} [10], Xe^0 - O^{2-} [11], La^{3+} - O^{2-} [12] fission product interactions with UO_2. For the pure UO_2 case, separate sets of simulations using the Basak potential [13] were also carried out. The Basak potential is comprised of a Buckingham term plus a Morse term. For computational efficiency, the Wolf summation [14] is used to compute the long-range Coulombic interactions.

The computational supercells were initially set to the optimized lattice constant 0.5469 nm (0.5456 nm in the Basak potential case). NPT (constant number, constant pressure, and constant temperature) simulations were carried out to determine the thermal expansions at different temperatures. The supercell dimensions were averaged over 100 ps, and the thermal expansion strains are 0.001865 (0.003004), 0.003803 (0.006231), 0.005827 (0.009728), 0.007905 (0.013508), 0.010089 (0.017626) at 300, 600, 900, 1200, and 1500 K for Buckingham (or Basak) potential. All thermal conductivity MD simulations were carried out with the thermal expansion taken into account.

To fit the temperature profiles, a least-squares fit for the linear regression is used. The temperature profiles were fitted in the ranges $w < z < L_z/2 - w$, and $L_z/2 + w < z < L_z - w$, with the choice of the excluded width w as 0.26, in agreement with earlier studies [15]. The obtained gradients from left and right slopes in the temperature profiles are then averaged to determine the thermal conductivity.

3. Results and discussions

MD simulations of pure UO_2 are carried out using both Buckingham potential and Basak potential, at 100, 200, 300, 600, 900, 1200, and 1500 K. At each temperature, a set of simulations at different lengths were included, 19, 24, 32, 49, and 65 nm.

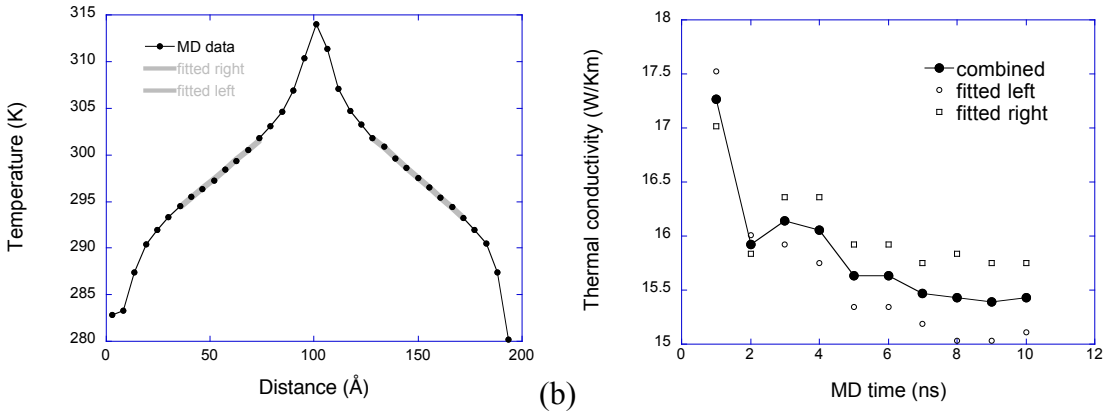

(a) (b)

Figure 2. (a) Averaged temperature profile at 300 K, with sample length of 19 nm, for MD simulations of 10 ns. Least-squares fits of the linear regression are also shown. (b) Thermal conductivity result at 300 K for the same sample in (a).

In Figure 2a, a typical temperature profile from MD simulations is shown. This temperature profile is averaged over an MD time of 10 ns, for a sample length of 19 nm at 300 K. The corresponding thermal conductivity as computed from Eq. 1 is shown in

Figure 2b, as a function of different MD run time, from 1 – 10 ns. From Figure 2b, it is noted that an MD simulation time of about 5 ns is needed for the thermal conductivity to reach the converged value [16].

More accurate determination of the thermal conductivity by allowing extensive MD run time of ~ 10 ns provides a solid basis for extrapolation of the MD results to the value for an infinitely large system. In the relatively short supercells used in the current MD simulation setups, a fairly significant portion of phonons propagate ballistically through the system due to relatively large phonon mean free path of the system, but scatter from the hot and cold plates. This causes the thermal conductivity obtained from MD simulations to be lower than they should be, especially at low temperature. The conventional method to extrapolate the value to an infinitely large system is based on a linear formula,

$$\frac{1}{\kappa} = \frac{1}{\kappa_\infty} + \frac{c}{L_z} \tag{4}$$

where c is a constant related to scattering by the hot and cold plates, L_z is the length of the simulation cell and κ_∞ is the thermal conductivity for a simulation cell of infinite length. As shown in our recent work [17], we found that a quadratic correction is sometimes needed in order to take non-linear effect in the UO_2 lattice into account, which brings the fitting formula to a more general one,

$$\frac{1}{\kappa} = \frac{1}{\kappa_\infty} + \frac{c_1}{L_z} + \frac{c_2}{L_z^2} \tag{5}$$

where c_1 and c_2 are both constants.

In Figure 3, MD results for the computed thermal resistivity κ^{-1} vs. inverse sample length L_z^{-1} for UO_2 employing Buckingham potential, at 300 and 1200 K are shown. The lines are fits to the MD data using Eq. 5. From Figure 3, it is shown that the MD data at 300 K suggests a strong quadratic correction. Also, the extrapolated value to the infinite length, κ_∞, 27.3 W/Km is significantly larger than the MD obtained data, 24.8 W/Km at the largest sample with 65 nm in length. This difference is substantially increased for even lower temperatures (not shown). However, at much higher temperature, 1200 K, such non-linear correction is weak. At this temperature, the extrapolated value to the

infinite length, κ_∞, 7.6 W/Km is only slightly larger than the MD obtained data, 7.2 W/Km at the 65 nm sample.

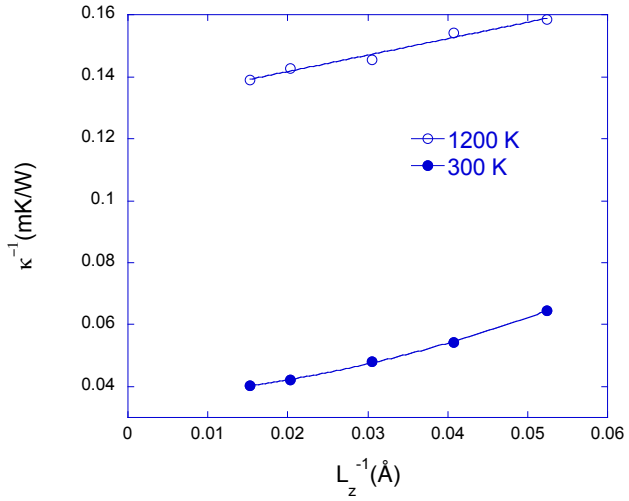

Figure 3. MD results for the computed thermal resistivity κ^{-1} vs. inverse sample length L_z^{-1} for UO_2 employing Buckingham potential, at 300 and 1200 K. The lines are fits to the MD data using Eq. 5.

The thermal conductivity κ_∞ for UO_2, extrapolated from MD results at different sample lengths using the above methodology, is shown in Figure 4, at different temperatures. Both sets of κ_∞ data, employing Buckingham potential and the Basak potential, are shown. The results from Buckingham potential are higher than those from Basak potential for T > 100 K.

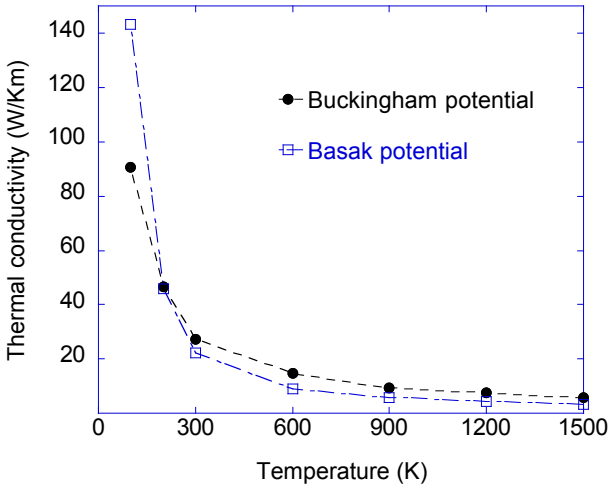

Figure 4. κ_∞ for UO_2 at different temperature using two potential models: Buckingham and Basak.

Next, fission products are incorporated into the supercells used for the thermal conductivity simulations. For Xe, the bound Schottky tri-vacancy is substituted into the supercell. For La, a single U vacancy is substituted. These are expected to be the energetically favored incorporation sites for the respective fission products [18]. The locations of the substitution sites are chosen according to a random distribution for the specified composition. Three compositions of fission products, 0.34, 0.71, and 1.03 atomic percent of Xe (La) are introduced to the UO_2 samples.

MD simulations were carried out for the UO_2 samples with fission products at 100, 300, 900, and 1500 K. The sample lengths used to determine the κ_∞ values are 19 nm, 38 nm, and 57 nm for the Xe cases. Since the impurity scattering from the Xe Schottky defects is strong, the length dependence for all Xe cases is weak. For the La cases, since the impurity scattering from La defects is much weaker, the length dependence is stronger, especially for cases with smaller La concentration. The sample lengths used to determine the κ_∞ values are similar to those in the Xe cases, except for the 0.34 % La case at 100 K where samples with length up to 76 nm are used.

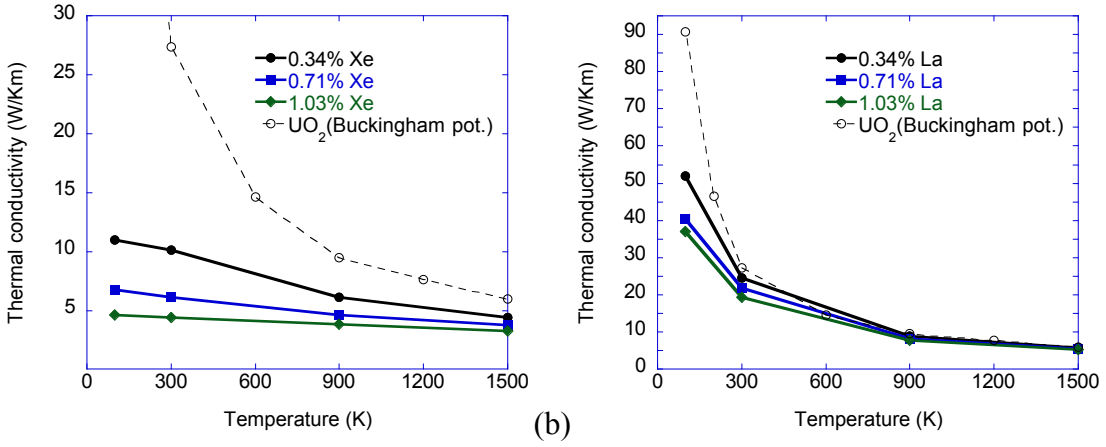

Figure 5. κ_∞ for UO_2 at different temperature (a) 0.34, 0.71, and 1.03 atomic percent Xe, (b) 0.34, 0.71, and 1.03 atomic percent La. κ_∞ for UO_2 at different temperatures obtained using the Buckingham potential is also plotted for comparison.

The thermal conductivity κ_∞ for UO_2 with the fission product Xe at concentrations of 0.34, 0.71, and 1.03 atomic percent is shown in Figure 5a at different temperatures, from 100 K and up to 1500 K, along with the results for pure UO_2. The strong phonon scattering by the Xe Schottky defects severely reduces the thermal conductivity, even at the lowest concentration of 0.34 atomic percent. For example, at

room temperature, the κ_∞ value changed from 27.3 W/Km to merely 10.2 W/Km in the 0.34% Xe case. Similar plots of κ_∞ for UO_2 with the fission product La is shown in Figure 5b, suggesting much weaker scattering. For example, also at room temperature, the κ_∞ value ranges from 24.6 to 19.4 W/Km for La concentrations from 0.34 to 1.03 atomic percent. These values are much higher than the Xe cases at the same temperature.

4. Correcting phonon-spin scattering not captured by the MD simulations

The MD simulations for pure UO_2 overestimate the thermal conductivity compared to experiments, especially at low temperature, see Figure 6a. As recently shown, this is due to resonant scattering of phonons by spins in the paramagnetic phase of UO_2 [17], which is not captured by the MD simulations. However, we can correct this deficiency by using the phonon-spin scattering contribution (labeled phonon-magnetic scattering in Figure 6) derived from experimental data [17]. The phonon-spin scattering relaxation time is derived from the experimental data shown in Figure 6a by fitting the data points to the Callaway model [19] including a term for the phonon-spin scattering. This relaxation time is then added to the total relaxation time derived for the MD results using the same Callaway model, but obviously without the phonon-spin contribution. As shown in Figure 6a, this approach significantly improves the agreement with experiments for pure UO_2. We can apply the same methodology to correct the MD predictions for UO_2 containing fission products. The results are shown in Figure 6b and in Figure 7. The general conclusions presented above for the impact of fission products on UO_2 thermal conductivity are still valid, but the overall conductivity is significantly reduced by including phonon-spin scattering, in particular at low temperatures (compare Figure 5 and 7).

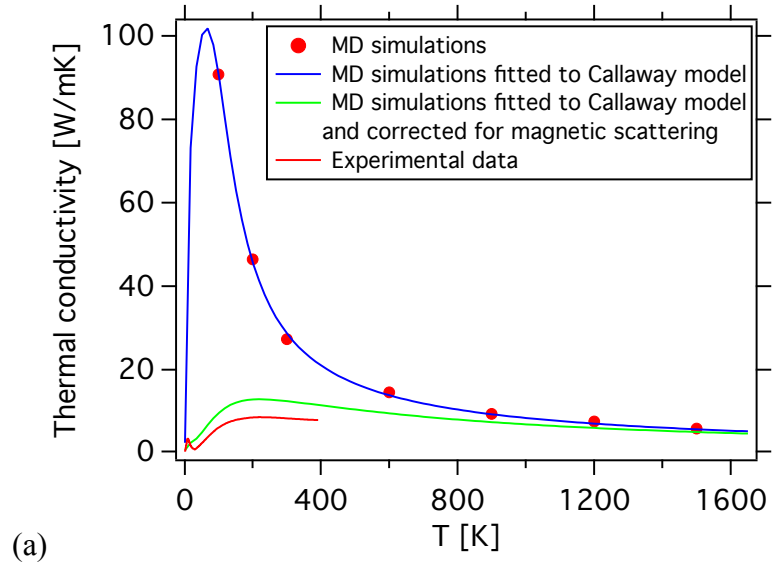

(a)

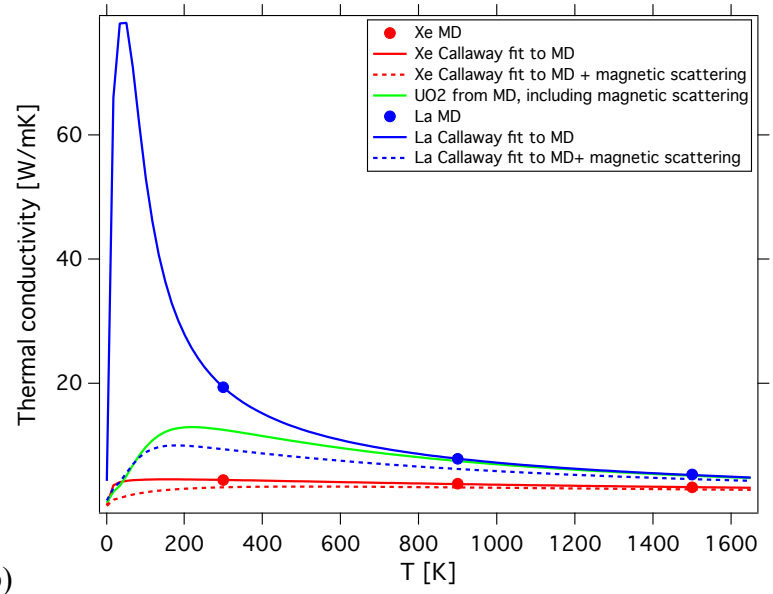

(b)

Figure 6. (a) MD simulation of the UO_2 thermal conductivity, both with and without correction for spin-phonon scattering. The spin-phonon scattering correction was derived by fitting a Callaway model to the experimental data [17] and then adding the spin-phonon relaxation time to the MD results. (b) MD simulation of the impact of 1% Xe atoms or La ions on the UO_2 thermal conductivity, both with and without correction for spin-phonon scattering. The spin-phonon scattering correction was derived by fitting a Callaway model to the experimental data [17] and then adding the spin-phonon relaxation time to the MD results.

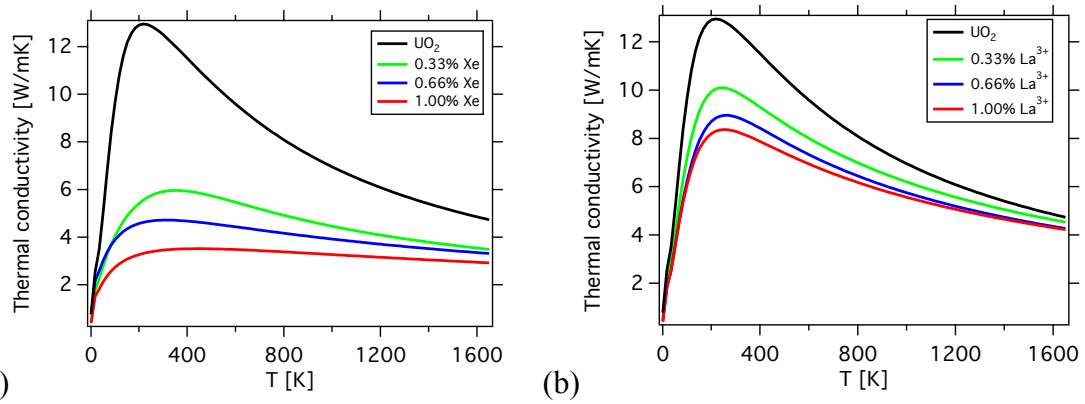

Figure 7. (a) Reduction of UO_2 thermal conductivity by Xe atoms, including correction for spin-phonon scattering. These results were obtained from the data in Figure 5 by adding the spin-phonon scattering contribution derived from experimental data. (b) Reduction of UO_2 thermal conductivity by La ions, including corrections for spin-phonon scattering. These results were obtained from the data in Figure 5 by adding the spin-phonon scattering contribution derived from experimental data.

4. Summary

In summary, MD simulations were carried out to determine quantitatively, the effect of two fission products, Xe and La, on the thermal conductivity of UO_2, as a function of the fission product concentration, for a range of temperatures, 100 – 1500 K. Accurate determination of the thermal conductivity was achieved by using extensive MD run times of ~ 10 ns, which provides a solid basis for extrapolation of the MD results to values for an infinitely large systems. The strong phonon scattering by Xe Schottky defects severely reduces the thermal conductivity, while the thermal conductivity for UO_2 with the fission product La exhibits much weaker scattering. Finally, the phonon-spin scattering not captured by the MD simulations is corrected through fitting the experimental data to the Callaway model including a term for the phonon-spin scattering.

References

[1] T. Watanabe, S.B. Sinnott, J.S. Tulenko, R.W. Grimes, P.K. Schelling, S.R. Phillpot, Thermal transport properties of uranium dioxide by molecular dynamics simulations, Journal of Nuclear Materials, 375 (2008) 388-396.

[2] M.R. Tonks, P.C. Millett, P. Nerikar, S. Du, D. Andersson, C.R. Stanek, D. Gaston, D. Andrs, R. Williamson, Multiscale development of a fission gas thermal conductivity model: Coupling atomic, meso and continuum level simulations, Journal of Nuclear Materials, 440 (2013) 193-200.
[3] P. Jund, R. Jullien, Molecular-dynamics calculation of the thermal conductivity of vitreous silica, Physical Review B, 59 (1999) 13707-13711.
[4] F. MullerPlathe, A simple nonequilibrium molecular dynamics method for calculating the thermal conductivity, J Chem Phys, 106 (1997) 6082-6085.
[5] T. Ikeshoji, B. Hafskjold, Nonequilibrium Molecular-Dynamics Calculation of Heat-Conduction in Liquid and through Liquid-Gas Interface, Mol Phys, 81 (1994) 251-261.
[6] X.W. Zhou, S. Aubry, R.E. Jones, A. Greenstein, P.K. Schelling, Towards more accurate molecular dynamics calculation of thermal conductivity: Case study of GaN bulk crystals, Physical Review B, 79 (2009).
[7] http://lammps.sandia.gov.
[8] G. Busker, A. Chroneos, R.W. Grimes, I.W. Chen, Solution mechanisms for dopant oxides in yttria, J Am Ceram Soc, 82 (1999) 1553-1559.
[9] R.W. Grimes, Solution of Mgo, Cao, and Tio2, in Alpha-Al2o3, J Am Ceram Soc, 77 (1994) 378-384.
[10] R.W. Grimes, C.R.A. Catlow, The Stability of Fission-Products in Uranium-Dioxide, Philos T R Soc A, 335 (1991) 609-634.
[11] R.G.J. Ball, R.W. Grimes, Diffusion of Xe in Uo2, J Chem Soc Faraday T, 86 (1990) 1257-1261.
[12] L. Minervini, Atomistic Simulations of Defective Oxides, Ph.D. thesis, Imperial College (2000).
[13] C.B. Basak, A.K. Sengupta, H.S. Kamath, Classical molecular dynamics simulation of UO2 to predict thermophysical properties, Journal of Alloys and Compounds, 360 (2003) 210-216.
[14] D. Wolf, P. Keblinski, S.R. Phillpot, J. Eggebrecht, Exact method for the simulation of Coulombic systems by spherically truncated, pairwise r(-1) summation, J Chem Phys, 110 (1999) 8254-8282.
[15] P.C. Howell, Thermal Conductivity Calculation with the Molecular Dynamics Direct Method I: More Robust Simulations of Solid Materials, J Comput Theor Nanos, 8 (2011) 2129-2143.
[16] Considering MD time step of 1 fs, this equivalents to 5 million MD steps.
[17] K. Gofryk et al., in press, Nature Commun.
[18] X.Y. Liu, D.A. Andersson, B.P. Uberuaga, First-principles DFT modeling of nuclear fuel materials, J Mater Sci, 47 (2012) 7367-7384.
[19] J. Callaway, Model for Lattice Thermal Conductivity at Low Temperatures, Phys Rev, 113 (1959) 1046-1051.